2007 IEEE International Conference on
Robotics and Automation
Roma, Italy, 10-14 April 2007

Visual-based Impedance Force Control of Three-dimensional Cell Injection System

Haibo Huang, Dong Sun, James K. Mills, and Wen J. Li

Abstract—**Biological cell injection is laborious work which requires lengthy training and suffers from a low success rate. Even a tiny excessive manipulation force can destroy the membrane or tissue of the biological cell. This makes the control of the injection force an important factor in the cell injection process. In this paper, a vision-based impedance force control algorithm is proposed based on dynamic modeling of a laboratory test-bed injection system. The injection force is calibrated in a cell injection task to derive the relationship between the force and the cell deformation. A cell biomembrane point-load model is utilized in this force calibration. In three-dimensional cell injection task, the total cell membrane deformation is estimated, based on the $X-Y$ coordinate frame deformation of the cell, as measured with a microscope, and the known angle between the injector and the $X-Y$ plane. Further, a relationship between the injection force and the injector visual displacement of the cell membrane is derived. Based on this force visual estimation scheme, an impedance force control algorithm is developed. Finally, experimental results are given which demonstrate the effectiveness of the proposed approach.**

I. Introduction

Since its invention, biological cell injection has been widely applied in gene injection [1], in-vitro fertilization (IVF) [2], intracytoplasmic sperm injection (ISCI) [3,4] and drug development [5]. Existing commercial cell injection solutions have been unable to fulfill the expectations of the industry. Most cell injection operations are still performed manually. Studies indicate that skilled operators require up to one year of training and can achieve only about 15% success rate during the entire transgenic task (gene injection into cells) [6]. In addition, most manual cell injection processes are neither accurate nor repeatable. Hence, there exists an increasing demand for an accurate and reliable cell injection system and methodology so that large batch biomanipulation production can be realized automatically.

During the process of cell injection, the injection force is an important factor that affects the survivability of the injected cells. Proper detection and control of the cell injection force helps to improve the performance of cell injection systems. Limited research has been performed to determine the forces involved in the cell injection. Research on bonding a microinjection pipette on the tip of a PVDF sensor to detect the injection forces in fish egg biomanipulation was performed in [6-10]. Sun *et al.* [11] developed a MEMS-based two-axis cellular force sensor to investigate the mechanical properties of mouse oocyte zona pellucida (ZP). Zhang *et al.* [12] developed a micrograting-based injection force sensor with a surface micromachined silicon-nitride injector. These force sensors, however, could not get the real-time force feedback, and the introduction of force sensors adds complexity to the system.

In this paper, a new cell injection system with force control is developed for cell injection tasks. Injection force is calibrated first in horizontal cell injection tasks to derive the relationship between the force and the cell deformation. A cell biomembrane point-load model [11] is utilized in such force calibration. Further, since the cell deformation is generally difficult to be measured directly in three dimentional injection tasks, a relationship between the injection force and the injector visual displacement inside the cell is derived for easy implementation. With the estimated injection force, an impedance force control strategy is then developed, in a similar manner to [13]. Injector motion planning is also designed in this study. Finally, experiments are performed to demonstrate the effectiveness of the proposed approach. The major contributions of this work are threefold. First, we propose a new methodology to use planar visual feedback to estimate 3D cell deformation and injection force. Second, we propose an automatic motion planning methodology designed for cell injection tasks. Third, we propose to use an impedance force control algorithm to regulate the injection force during the cell injection.

II. System Setup

Fig. 1 illustrates the newly developed cell injection system in our laboratory. The system is mainly comprised of an executive module, a sensory module and a control module [14]. The executive module consists of $X-Y-\theta$ positioning table and the injection manipulator mounted on the Z -axis. The cells are placed and fixed on the working plate. The coordinate motion between the $X-Y-\theta$ table and the *Z*-axis injector is needed to perform the cell injection

This work was supported by a grant from Research Grants Council of the Hong Kong Special Administrative Region, China [Reference. No. CityU 119705].

H. B. Huang and Dong Sun are with the Department of Manufacturing Engineering and Engineering Management, City University of Hong Kong, Kowloon, Hong Kong (e-mail: {hbhuang,medsun}@cityu.edu.hk).

J. K. Mills is with the Department of Mechanical and Industrial Engineering, University of Toronto, ON M5S 3G8 Canada (email: mills@mie.utoronto.ca).

Wen J. Li is with the Centre for Micro and Nano System, the Chinese University of Hong Kong, Shatin, NT, Hong Kong (email: wen@acae.cuhk.edu.hk).

task. The $X-Y$ stage has a workspace of 60mm×60mm, with an accuracy of 0.3 μm. The Z-axis stage has a workspace of 50mm, with an accuracy of 0.3 μm. The injector pipette has a fixed angle known by φ with respect to the $X-Y$ plane. The X, Y, and Z axes are driven by DC brushless motors with embedded encoder to measure the position information. The sensory module mainly contains a vision system that includes four parts: optical microscope, CCD camera, PCI image capture and processing card, and image processing computer. The PULNIX TM-6701AN Progressive Scan camera and the NI 1409 image capture card have a high image capture frequency of 60Hz to observe the cell injection process. The control module consists of a host computer (PD 2.8GHz) and a DCT0040 motion control/drive system provided by DynaCity Technology (HK) Ltd. [15].

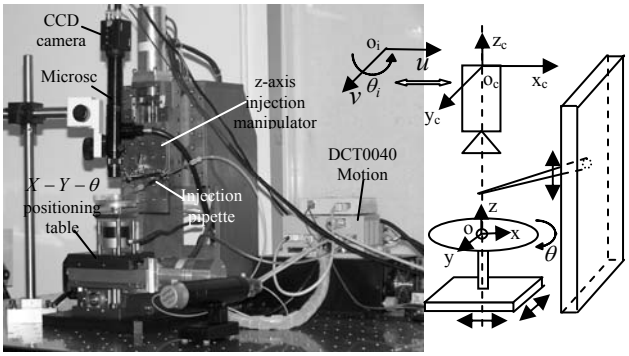

Fig. 1. Setup and configuration of a laboratory test-bed cell injection system.

III. System Modeling

Fig. 1 illustrates the configuration of the developed microinjection system. Define $o-xyz$ as the coordinate frame whose origin o is located at the center of the working plate. Define $o_c-x_cy_cz_c$ as the camera coordinate frame, where o_c is located at the center of the camera, and z_c coincides with the optical axis of the microscope. Define o_i-uv as the coordinate frame in the image plane, with three coordinates u, v and the rotational angle θ_i. The origin o_i is located in the optical axis, and the axes u and v are within the camera image plane perpendicular to the optical axis.

In a similar way [16], the relationship between the camera coordinates $[X_c,\ Y_c,\ Z_c,\ \theta_c]^T$ and the stage coordinates $[X,\ Y,\ Z,\ \theta]^T$ is given as:

$$\begin{bmatrix} X_c \\ Y_c \\ Z_c \\ \theta_c \end{bmatrix} = \begin{bmatrix} R & 0 \\ 0 & 1 \end{bmatrix} \begin{bmatrix} X \\ Y \\ Z \\ \theta \end{bmatrix} + \begin{bmatrix} d \\ 0 \end{bmatrix} \tag{1}$$

where $R = \begin{bmatrix} \cos\alpha & \sin\alpha & 0 \\ -\sin\alpha & \cos\alpha & 0 \\ 0 & 0 & 1 \end{bmatrix} \in \Re^{3\times 3}$ is the rotation matrix from the frame $o-xyz$ to the frame $o_c-x_cy_cz_c$, α is the angle between the two frames, and $d=[d_x,\ d_y,\ d_z]^T$ denotes the displacement between origins of the two frames. Since the two frames are fixed, both R and d are constant.

The relationship between image coordinates $[u,\ v,\ \theta_i]^T$ and camera coordinates $[X_c,\ Y_c,\ Z_c,\ \theta_c]^{\mathrm{T}}$ is:

$$\begin{bmatrix} u \\ v \\ Z \\ \theta_i \end{bmatrix} = \begin{bmatrix} f_x & 0 & 0 & 0 \\ 0 & f_y & 0 & 0 \\ 0 & 0 & 1 & 0 \\ 0 & 0 & 0 & 1 \end{bmatrix} \begin{bmatrix} X_c \\ Y_c \\ Z_c \\ \theta \end{bmatrix} - \begin{bmatrix} 0 \\ 0 \\ d_z \\ 0 \end{bmatrix} \tag{2}$$

where $f_x = \lambda/\delta_{\mathrm{u}}$ and $f_y = \lambda/\delta_{\mathrm{v}}$ are the display resolutions of the vision system in the two coordinate directions, λ is the magnification factor of the microscope objective, δ_{u} and δ_{v} are the u-axis and v-axis intervals between CCD pixels. The image coordinate vector in (2) is augmented from 3×1 to 4×1 by adding the coordinate Z for easy processing later.

Substituting (1) into (2) yields a relationship between coordinates $[u,\ v,\ Z,\ \theta_i]^T$ and $[X,\ Y,\ Z,\ \theta]^T$:

$$\begin{bmatrix} u \\ v \\ Z \\ \theta_i \end{bmatrix} = T \begin{bmatrix} X \\ Y \\ Z \\ \theta \end{bmatrix} + \begin{bmatrix} f_x d_x \\ f_y d_y \\ 0 \\ 0 \end{bmatrix} \tag{3}$$

where $T = \begin{bmatrix} f_x\cos\alpha & f_x\sin\alpha & 0 & 0 \\ -f_y\sin\alpha & f_y\cos\alpha & 0 & 0 \\ 0 & 0 & 1 & 0 \\ 0 & 0 & 0 & 1 \end{bmatrix}$ is the transformation matrix between the image frame and the stage frame. Since the both frames are fixed, T is time-invariant.

Using Lagrange's equation of the motion, the dynamics of the four DOF motion stage is given as

$$\begin{bmatrix} m_x+m_y+m_p & 0 & 0 & 0 \\ 0 & m_y+m_p & 0 & 0 \\ 0 & 0 & m_z & 0 \\ 0 & 0 & 0 & I \end{bmatrix} \begin{bmatrix} \ddot{X} \\ \ddot{Y} \\ \ddot{Z} \\ \ddot{\theta} \end{bmatrix} + \mathrm{N}' \begin{bmatrix} \dot{X} \\ \dot{Y} \\ \dot{Z} \\ \dot{\theta} \end{bmatrix} + \begin{bmatrix} 0 \\ 0 \\ -m_z g \\ 0 \end{bmatrix} = \tau - \begin{bmatrix} f_e \\ 0 \end{bmatrix} \tag{4}$$

where m_x, m_y and m_z are masses of the X, Y and Z positioning tables, m_p is the mass of the working plate, I_p is the inertia of the rotational axis and the working plate, $N'\in\Re^{4\times 4}$ denotes a diagonal matrix of the positioning table that reflects damping and viscous friction

effects, $\tau = [\tau_x, \ \tau_y, \ \tau_z, \ \tau_r]^T$ denotes the torque inputs to the driving motors, and $f_e = [f_{ex}, \ f_{ey}, \ f_{ez}]^T$ is the external force applied to the actuators during the cell injection. During the cell injection process, the rotation axis θ does not change such that only $[f_{ex}, \ f_{ey}, \ f_{ez}]^T$ is considered. Note that $f_e = 0$ if the injector does not contact the cells.

Define $q = [u, \ v, \ Z, \ \theta_i]^T$ as the generalized coordinate. Substituting (3) into (4) yields the following dynamics equation in terms of q :

$$M\ddot{q} + N\dot{q} + G = \tau - \begin{bmatrix} f_e \\ 0 \end{bmatrix} \tag{5}$$

IV. Injection Controller

4.1 Motion Planning

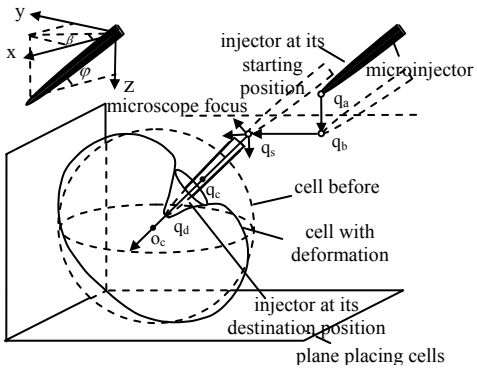

Fig. 2. Three-dimensional cell injection process

A suitable injection motion plan must be designed for three-dimensional cell injection tasks. Fig. 2 illustrates a cell injection process proposed in this study. The absolute height of the working plate that the cells are placed on must be precisely calibrated. When the tilt angle of the injector φ is fixed, the path the injector follows can be designed as shown in Fig. 2. Denote q_a as the position of head of the injector at the beginning of manipulation. The injector moves to the starting injection height that is in the focal range of the microscope, and stops at the position q_b . The movement of the injector and deformation of the cell membrane in the $X-Y$ plane can now be observed by the microscope. The image-based visual servoing methodology is used to guide the injector towards the starting injection position q_s . To ensure that the injector points toward the centre of the cell denoted by o_c , the X -, Y -, and Z - axes need to move simultaneously. The so-called pre-piercing step is then initiated by accelerating the injector to approach the cell. When the injector reaches the position q_c , which locates the surface of the cell membrane, the velocity is designed to be the highest since a sufficiently high injection velocity is needed at this moment to pierce the cell. Next, the injector is decelerated to approach the desired injection position q_d . After injecting the genes into the cell at q_d , the injector is accelerated in the opposite direction, to be pulled out of the cell membrane. The velocity and acceleration profiles of the injector, starting from the pre-piercing step at q_s and ending at the pulling out step at the same q_s , are shown in Fig. 3.

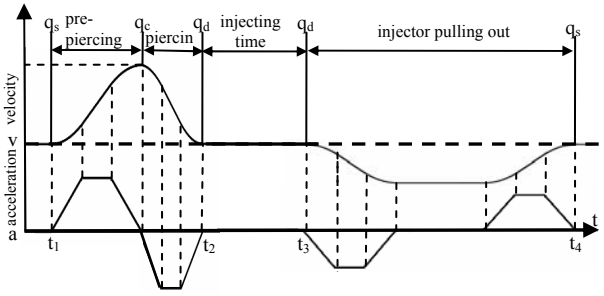

t_1–at q_s of starting injection position; t_2– at q_d before injecting time; t_3–at q_d after injecting time; t_4– at q_s after injector pulling out.

Fig. 3. Velocity and acceleration profiles of injector in injection process.

4.2 Cell Injection Force Estimation

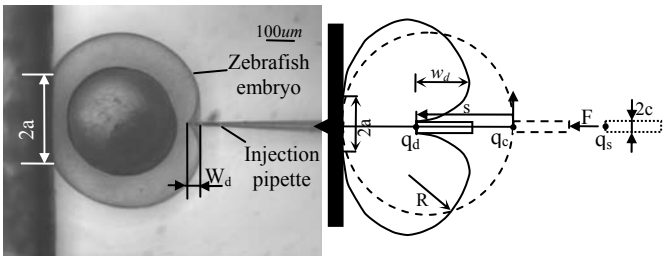

Fig. 4. Horizontal cell injection force calibration with cell biomembrane point-load model..

During the three-dimensional cell injection process, the geometric change of the cell biomembrane in Z -axis cannot be detected by the microscope. To solve this problem, we propose to utilize the deformation of the cell, as observed in the $X-Y$ plane, to estimate the total cell membrane deformation. This method is valid under the condition that the angle between the Z-axis injector pipette and the $X-Y$ plane is known, and also, the batches of cells have the same membrane dynamic characteristics.

Experiments of cell injection with the injector placed in the $X-Y$ plane are conducted first for calibration purposes, as shown in Fig. 4. The cell injection force can be estimated using the biomembrane point-load model [11] shown in Fig. 4. The pipette with radius c exerts a force F on the membrane, creating a dimple with a radius a and depth w_d and semicircular curved surface with a radius R . The cell injection force can be calculated as [11]:

$$F = \frac{2\pi Eh\, w_d^{\,3}}{a^2(1-\gamma)}\left[\frac{3-4\zeta^2+\zeta^4+2\ln\zeta^2}{(1-\zeta^2)(1-\zeta^2+\ln\zeta^2)^3}\right] \tag{6}$$

where E is the membrane elastic modulus, γ is the Poisson ratio, h is the thickness of the biomembrane, and $\zeta = c/a$, c is the radius of the injector. In equation (6), biomembrane

material parameters E and γ and dimensions h and c are constants, a and w_d are variables obtained from images.

In practice, the parameter w_d is more difficult to obtain than the distance the injector has moved inside the undeformed cell membrane boundary, i.e. from q_c to q_d, denoted as s *in* Fig 4**.** Through calibration experiments and curve fitting, the fitted relationship of the cell injection force F to the injector moving distance inside the cell can be obtained. In a practical implementation, the injection force F can be determined given the distance the injector has moved inside the undeformed cell wall boundary, s, instead of w_d.

In a three-dimension injection, with the injector oriented at an angle φ relative to the $X-Y$ plane, the forces in the three axes can be derived as:

$$\begin{bmatrix} F_x \\ F_y \\ F_z \end{bmatrix} = F \cdot \begin{bmatrix} \cos(90^\circ - \varphi) \cdot \cos\beta \\ \cos(90^\circ - \varphi) \cdot \sin\beta \\ \sin(90^\circ - \varphi) \end{bmatrix} \tag{7}$$

where β is the angle between the injector and *x*-axis, both β and φ are fixed during the injection process. The distance of the injector inside the cell can be expressed as

$$s = \sqrt{(X - X_{qc})^2 + (Y - Y_{qc})^2 + (Z - Z_{qc})^2} \tag{8}$$

X_{qc}, Y_{qc} and Z_{qc} are coordinates at the contact point q_c as shown in Fig. 4, $\begin{bmatrix} X \\ Y \end{bmatrix} = T_{xy}^{-1} \begin{bmatrix} u - u_{qc} \\ v - v_{qc} \end{bmatrix}$, $[u, v]^T$ is the image coordinate of the pipette head and $[u_{qc}, v_{qc}]^T$ is the image coordinate of the point q_c. The deformation $Z - Z_{qc}$ cannot be detected by the microscope directly, which will be derived according to the deformations of *X*-axis and *Y* -axis. Thus, we rewrite equation (8) as:

$$s = \sqrt{(X - X_{qc})^2 + (Y - Y_{qc})^2 + \left(\frac{\sqrt{(X - X_{qc})^2 + (Y - Y_{qc})^2}}{\sin\varphi} \right)^2} \tag{9}$$

4.3 Hybrid Impedance Force Control in Cell Injection

Impedance control achieves the desired dynamics response of a system by controlling its impedance to a desired value and is robust to model uncertainties and external disturbance. A hybrid impedance control method that combines the impedance control and the vision-based injection force estimation will be developed here.

The contact space impedance force control is given as:

$$m\ddot{e} + b\dot{e} + ke = f_e \tag{10}$$

where m, b and k are the desired impedance parameters, $e = [X_d, \ Y_d, \ Z_d]^T - [X, \ Y, \ Z]^T$, representing the position errors of the $X-Y$ stage and the $Z-$ axis injector. The external force f_e applied to the actuator can be expressed as:

$$f_e = -[F_x \quad F_y \quad F_z]^T \tag{11}$$

We now solve for $[\ddot{X} \quad \ddot{Y} \quad \ddot{Z}]^T$ from (10) as follows:

$$\begin{bmatrix} \ddot{X} \\ \ddot{Y} \\ \ddot{Z} \end{bmatrix} = m^{-1} \left(m \begin{bmatrix} \ddot{X}_d \\ \ddot{Y}_d \\ \ddot{Z}_d \end{bmatrix} + b\dot{e} + ke - f_e \right) \tag{12}$$

Substituting (12) into (5) yields an image-based three-dimensional torque controller as follows:

$$\tau_{xyz} = M_{xyz} \left(\begin{bmatrix} \ddot{X}_d \\ \ddot{Y}_d \\ \ddot{Z}_d \end{bmatrix} + m^{-1}(b\dot{e} + ke - f_e) \right) + N_{xyz} \begin{bmatrix} \dot{X} \\ \dot{Y} \\ \dot{Z} \end{bmatrix} + G_{xyz} + f_e^d \tag{13}$$

where M_{xyz}, N_{xyz} and G_{xyz} are sub-matrices of M, N and G regarding to X, Y and Z axis, respectively, and f_e^d is the desired injection force that can be determined according to the desired injector moving distance inside the cell.

Substituting (13) into (5) yields a closed-loop equation:

$$M_{xyz} m^{-1} (m\ddot{e} + b\dot{e} + ke - f_e) = f_e - f_e^d \tag{14}$$

Substituting (10) into (14) leads to $f_e = f_e^d$.

V. EXPERIMENTS

Experiments were performed to verify effectiveness of the proposed approach. For simplicity, the rotation angle between the image frame and the stage frame is set to zero ($\alpha = 0^\circ$). The displacement between origins of the two frame is $d = [0, \ 0, \ 30mm]^T$. The magnification factor of the microscope objective is $\lambda = 30$. After system calibration, the modeling parameters M_{xyz}, N_{xyz} and G_{xyz} could be known [14]. The angle between the injector and the x-axis is $\beta = 45^\circ$. The angle between the injector and the $Z-$ axis is $\varphi = 35.26^\circ$. Thus, we could derive $f_e = \left[-\sqrt{3}/3 \ F, \ -\sqrt{3}/3 \ F, \ -\sqrt{3}/3 \ F \right]^T N$ from (7) and (11).

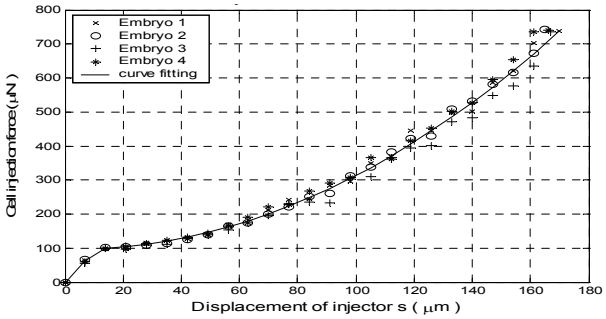

Fig. 5. Cell injection force calibration.

The cell to be selected for injection is the zebrafish embryo. Zebrafish is commonly chosen as an animal model in

biomanipulation because of its easily accessible eggs, short generation time, external fertilization and translucent embryos [7]. The diameter of the egg is approximately 600-700 μm . The Poisson ratio $\gamma = 0.5$. The thickness of the biomembrane $h = 3\mu m$, the radius of the injector $c = 6.4\mu$m , and the membrane elastic modulus $E = 1.51\ MPa$.

First, a series of calibration experiments were performed to obtain the relationship between the cell injection force F and the injector distance s inside the cell. The calibration experiments were performed by injecting the cell with the injector located in the $X-Y$ plane, as shown in Fig. 4. Fig. 5 illustrates the experimental results obtained with four embryos, based on which the cell injection force F can be directly estimated from the injector distance s instead of the cell biomembrane deformation w_d . Through curve fitting the relationship between the cell injection force and the injector distance s , the injection force F can be estimated as:

$$F = \begin{cases} 8.5714s & 7\mu m > s > 0 \\ 0.02274 \cdot s^2 - 0.09252 \cdot s + 95.31 & 170\mu m > s > 7\mu m \\ 0 & s > 170\mu m \end{cases} \quad (15)$$

Since the zebra fish embryo can be punctured after the distance s exceeds about 170 μm , in our experiments, the desired injection distance and desired pre-piercing movement distance are all 175 μm .

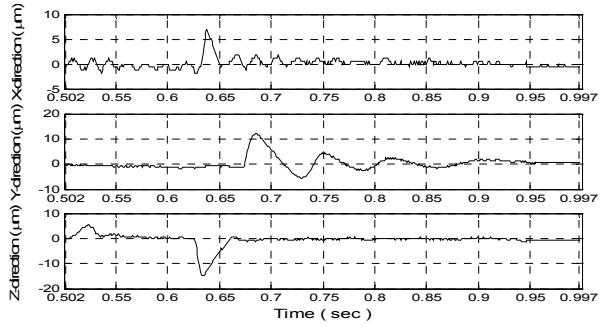

(a) Position error of injector in three axes;

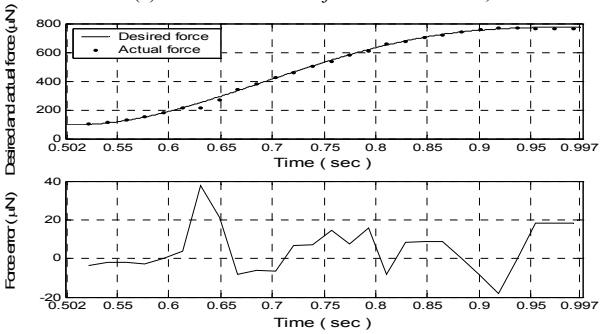

(b) Injection force and injection force error;

Fig. 6. Experimental results with the PID control.

The desired velocity and position profiles of the injector was in terms of Fig. 3. The total distance that the injector moved during the pre-piercing $(0\sec < t < 0.502\sec)$ and piercing period $(0.502\sec < t < 0.997\sec)$ was 350 μm . The injector moved 175 μm during the acceleration phase of motion, and reached its maximum cell injection velocity, 700 $\mu m / s$ when it contact the cell membrane. The injector was then decelerated and pierces the cell membrane, moving 175 μm within the cell. 2 seconds were needed to for injection and then the injector moved in the opposite direction to be pulled out of the cell $(3.00\sec < t < 5.23\sec)$. During the injector pulling out period, the injector moved more slowly than that during the piercing period, where the maximum velocity was 233 um / s .

In the experiments, three different control methods were used for comparison purposes. The embryo cells in the experiments were all collected in accordance with the standard embryo preparation procedures. None of the cells were used beyond one to two hours after fertilization, and all cells were of a similar size to each other. These conditions ensured that the assumption that all embryo cells used in our experiments exhibited the same dynamic characteristics is valid. The experimental results during the piercing period of the injection process ($0.502\sec < t < 0.997\sec$) are shown here. Fig. 6(a) illustrates the position errors of the injector in three axes with traditional PID control. The PID control gains were chosen as $k_p = diag\{6.299,\ 6.299,\ 7.244\}\ A/\mu m$, $k_d = diag\{1.575,\ 1.260,\ 1.575\}(A \cdot ms)/\mu m$, and $k_i = diag\{0.315,\ 0.378,\ 0.409\}\ A/(\mu m \cdot ms)$. As seen from the results, the largest trajectory error is about 15 μm after combining errors of three axes. Fig. 6(b) shows the injection force and force error. The largest force error is shown to exceed 35 μN .

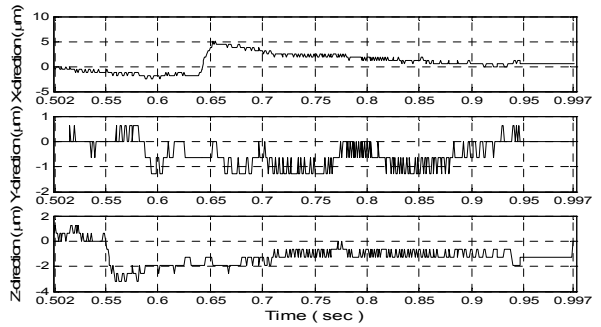

(a) Position error of injector in three axes;

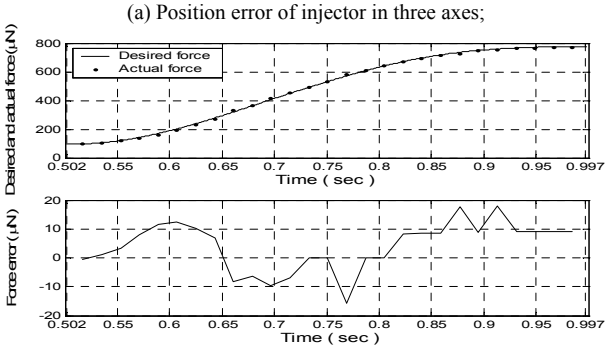

(b) Injection force and injection force error;

Fig. 7. Experimental results with the computer torque control.

Fig. 7(a) illustrates the position errors of the injector in three axes with the proposed controller without vision-based

force feedback. The controller in this case is equivalent to a computer torque control. The control gains are:

$$m = diag\{0.330,\quad 0.165,\quad 0.1635\}\,N/(\mu m \cdot ms^{-2}),$$

$$b = diag\{7.143,\quad 4.763,\quad 5.191\}\,N/(\mu m \cdot ms^{-1}),$$

$$k = diag\{9.049,\quad 7.144,\quad 10.855\}\,N/\mu m.$$

Experimental results show that the largest trajectory error was reduced to about 6 μm. Fig. 7(b) shows the injection force and the force error. It is seen that the maximum force error was reduced to about 18 μN.

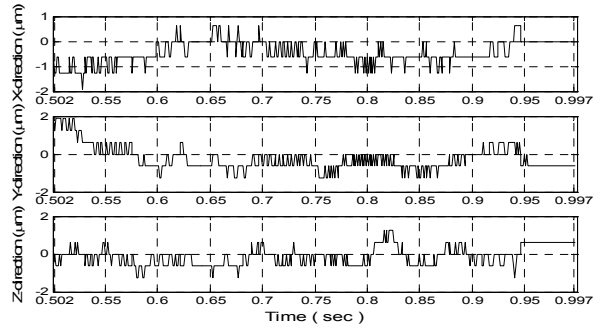

(a) Position error of injector in three axes;

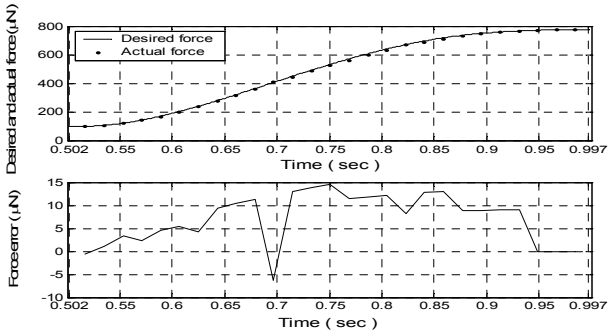

(b) Injection force and injection force error;

Fig. 8. Experimental results with the vision-based impedance force control.

Fig. 8(a) illustrates the position errors of the injector in three axes with the proposed vision-based impedance force control. The external force applied to the cell during the injection process could be regulated with the vision-based force feedback in the controller. The largest trajectory error was reduced to about 2 μm, as shown in Fig. 8(a). Fig. 8(b) illustrates the visual force feedback during the piercing period based on visual observation and the maximum force error was reduced to about 14 μN. It is clear to see that the proposed visual based impedance force control exhibits the best motion performance amongst all three control methods.

VI. Conclusions

In this paper, a microrobotic cell injection system with vision-based force control methodology is developed for biomanipulation. Injection force is calibrated first in a planar cell injection task to derive the relationship between the force and the cell deformation, where a cell biomembrane point-load model [11] is utilized. Further, since the cell deformation is generally difficult to measure directly in an out-of-plane injection tasks, a relationship between the injection force and the injector visual displacement inside the cell is derived for easy implementation. With the estimated injection force, an impedance force control strategy is then developed. An injection motion planning methodology is also proposed in this study. Finally, the effectiveness of the proposed approach is demonstrated by experiments.

References

[1] J. Kuncova and P. Kallio, "Challenges in Capillary Pressure Microinjection", Proc. IEEE Int. Conf. of EMBS, pp. 4998-5001, 2004.

[2] Y. Sun and B.J. Nelson, "Biological cell injection using an autonomous microrobotics system," The Int. Journal of Robotics Research, vol. 21, pp. 861-868, 2002.

[3] K. Yanagida, H. Katayose, H. Yazawa, Y. Kimura, K. Konnai and A. Sato, "The usefulness of a piezo-micromanipulator in intracytoplasmic sperm injection in humans," Human Reproduction, vol. 14, no. 2, pp. 448-453, 1998.

[4] K. K. Tan, D. C. Ng and Y. Xie, "Optical intra-cytoplasmic sperm injection with a piezo micromanipulator," The 4th World Congress on Intelligent Control and Automation, pp. 1120-1123, 2002.

[5] T. Nakayama, H. Fujiwara, K. Tastumi, K. Fujita, T. Higuchi and T. Mori, "A new assisted hatching technique using a piezo-micromanipulator," Fertility and Sterility, vol. 69, no. 4, 1998.

[6] A. Pillarisetti, W. Anjum, J. P. Desai, G. Friedman and A. D. Brooks, "Force feedback interface for cell injection," Proc. of the First Joint Eurohaptics Conf. and Symposium on Haptic Interfaces for Virtual Environment and Teleoperator Systems, 2005.

[7] A. Pillarisetti, M. Pekarev, A. D. Brooks and J. P. Desai, "Evaluating the role of force feedback for biomanipulation tasks," Symposium on Haptic Interfaces for Virtual Enviroment and Teleoperator Systems, pp.11-18, 2006.

[8] D. H. Kim, S. Yun and B. Kim, "Mechanical force sensor response of single living cells using a microrobotic system," Proc. IEEE Int. Conf. on Robotics and Automation, pp. 5013-5018, 2004.

[9] S. Y. Cho and Jae-Hong Shim, "A new micro biological cell injection system," Proc. IEEE Int. Conf. on Intelligent Robots and Systems, pp. 1642-1647, 2004.

[10] King W. C. Lai, Charlotte C. H. Kwong and Wen J. Li, "KL probes for robotic-based cellular nano surgery," Third IEEE Conf. on Nanotechnology, August 12, 2003.

[11] Y. Sun, K. T. Wan, K. P. Roberts, J. C. Bischof and B. J. Nelson, "Mechanical property characterization of mouse zona pellucida," IEEE/ASME Transactions on Nanobioscience, vol. 2, pp. 279-286, 2003.

[12] X.J. Zhang, S. Zappe, R.W. Bernstein, O. Sahin, C-C. Chen, M. Fish, M. Scott and O. Solgaard, "Integrated optical diffractive micrograting-based injection force sensor," The 12th Int. Conf. on Solid State Sensors, Actuators and Microsystems, pp. 1051-1054, 2003.

[13] D. Sun, and Y. H. Liu, "Modeling and impedance control of a two-manipulator system handling a flexible beam," ASME Journal of Dynamic Systems, Measurement, and Control, vol. 119, no. 4, pp. 736-742, December, 1997.

[14] H. B. Huang, D. Sun, J. K. Mills, and W. J. Li, "A visual impedance force control of a robotic cell injection system," Proc. IEEE Int. Conf. on Robotics and Biomimetics, pp. 233-238, Dec 2006.

[15] http://www.dynacitytech.com.

[16] W. Zhao, W.J. Zhang, M.M. Gupta, G.H. Zong and P.R. Ouyang, "A micro visual servo system for biological cell manipulation: overview and new developments," Proc. IEEE Int. Conf. on Control, Automation, Robotics And Vision, pp.429-434, 2002.